NJC

ROYAL SOCIETY OF CHEMISTRY

PAPER

View Article Online
View Journal

Cite this: DOI: 10.1039/d5nj03688g

Experimental and computational investigations of the products of halogenation of 1,2-chalcogenazole 2-oxides†

Phillip L. MacDougall, Mich W. Zeng, Jin Z. Wang, Peter C. Ho and Ignacio Vargas-Baca *

Received 16th September 2025,
Accepted 4th December 2025

DOI: 10.1039/d5nj03688g

rsc.li/njc

The halogenation reactions of 3-methyl-5-phenyl-1,2-tellurazole 2-oxide, benzo-1,2-selenazole 2-oxide and benzo-1,2-tellurazole 2-oxide were investigated in organic solution. The products were identified by single-crystal X-ray diffraction, and characterized by NMR, IR spectroscopies and mass spectrometry. The outcomes of the reactions resulted from one or more of three processes: (i) halogenation of the chalcogen, (ii) protonation, and (iii) halogenation of the heterocycle. Molecules in which the chalcogen was halogenated and protonated behaved as very weak Brønsted acids and displayed a strong affinity for bromide ions, crystallizing with tetraalkyl ammonium cations. In the case of benzo-1,2-selenazole 2-oxide, the heterocycle was chlorinated before the selenium atom. Chalcogen and hydrogen bonding are structural features that determine molecular arrangement in these crystals.

Introduction

Iso-tellurazole *N*-oxides (Scheme 1; **1**, **2**) stand out amongst organochalcogen-nitrogen heterocycles because of their ability to form well-defined, discrete, supramolecular aggregates[1–8] through Te···O chalcogen bonds (ChBs), the supramolecular interaction between electron-rich centers and the electrophilic region on the surface of a group-16 atom.[9] Interest in chalcogen bonding is undergoing fast expansion due to its proposed and demonstrated applications in crystal engineering,[10–15] organic semiconductors,[16] photoswitching,[17] organocatalysis,[18–21] anion sensing and transport across biological membranes.[22–24]

Early investigations revealed that solutions of **1** and **2** contain a mixture of macrocyclic tetramers ($\mathbf{1}_4$, $\mathbf{2}_4$) and hexamers ($\mathbf{1}_6$, $\mathbf{2}_6$) in equilibrium. Each of those aggregates can be isolated in solid form under specific crystallization conditions. In addition to the macrocycles, polymeric chains of iso-tellurazole *N*-oxides ($\mathbf{1}_\infty$) crystallize from media that only sustain low concentrations. Derivatives in which an aromatic bridge is formally inserted between the nitrogen and oxygen atoms (**3**, **4**, **5**) retain the ability to spontaneously assemble macrocyclic rings.[25]

Because Se···O ChBs are weaker than Te···O interactions, the behavior of the iso-selenazole *N*-oxides (**6**, **7**) is different at first glance. The two crystal structures in the literature consist of infinite chains in one case and a dimer formed by antiparallel chalcogen bonds in the other. However, ^{1}H VT-NMR experiments indicate that, at low temperature, **7** molecules aggregate into tetramers and hexamers.[4]

Energy decomposition analyses have shown that ChB interactions are stabilized by a combination of electrostatic, orbital, and dispersion contributions, and are countered by the Pauli repulsion.[2,26] The electrostatic component corresponds to the attraction between regions of the molecules that bear positive and negative electric potentials. The orbital contribution accounts for changes of electron density, both intra- and intermolecular, *i.e.* polarization and electron sharing or covalency. The London dispersion, arising from perturbational modelling of the interaction energy to second order, accounts for the interaction of each electron in one molecule or fragment with all the electrons in another. The steric or Pauli repulsion results from the interaction between closed shells of electrons, which requires occupation of antibonding orbitals, destabilizing the ChB interaction.[6]

Each of those factors suggests strategies to strengthen ChBs, which would be particularly useful in the case of selenium-centered ChBs. One straightforward approach would be increasing the electrophilicity of the chalcogen atom, for example by oxidizing the element with a halogen, as demonstrated in the case of tellurium with the chlorination of **1b** to form **1b**Cl_2 (Fig. 1), in principle.[7] DFT calculations showed that while V_{max} is indeed increased, there is a simultaneous decrease of electron density on the oxygen atom. Overall, **1b**Cl_2 is a better ChB

Department of Chemistry and Chemical Biology, McMaster University, 1280 Main Street West, Hamilton, Ontario, Canada L8S 4M1.
E-mail: vargas@chemistry.mcmaster.ca

† Dedicated to Professor Giuseppe Resnati, celebrating a career in fluorine and noncovalent chemistry on the occasion of his 70th birthday.

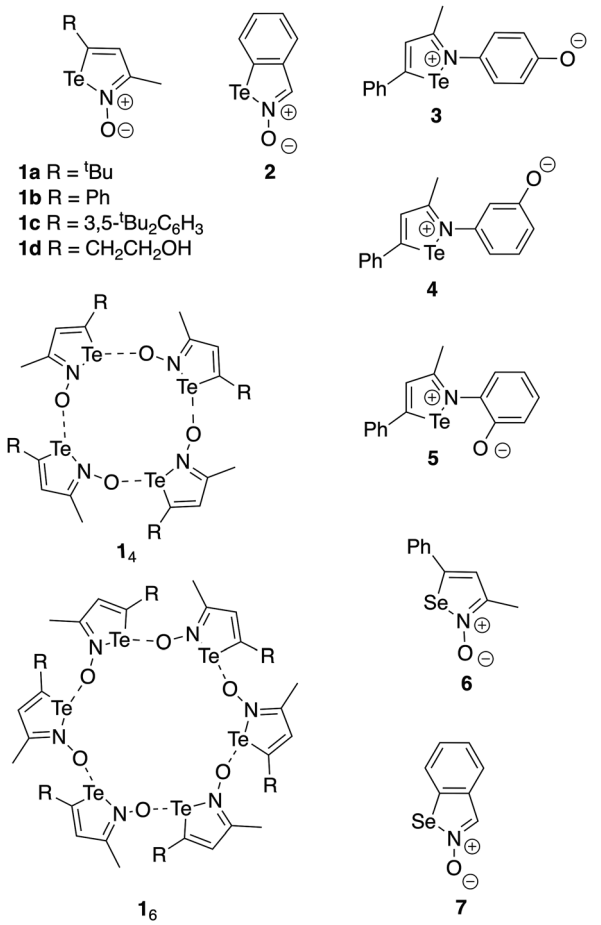

Scheme 1 Iso-Chalcogenazole derivatives discussed in this article.

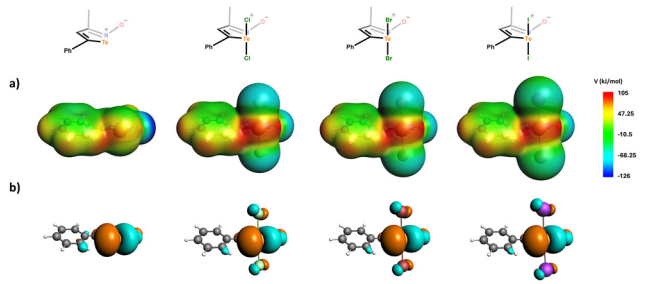

Fig. 1 DFT analysis of **1b**, **1b**Cl_2, **1b**Br_2, and **1b**I_2. (a) Electrostatic potential maps plotted on the 10^{-3} a.u. isodensity surface; (b) LUMOs (0.03 a.u. isosurfaces).

donor but a worse ChB acceptor than **1b**. Experimentally, it was shown that formation of ChB donor–acceptor interactions by rank of energy leads to the selective assembly of the **1b**$_2$(**1b**Cl_2)$_2$ macrocycle from mixtures of **1b** and **1b**Cl_2. These investigations have continued with the use of other halogens and the reactions of **2** and **7**, the results are summarized in this report. Given the interplay of experimental and computational work we employed, syntheses, structures, and calculations are presented interspersed and discussed in context.

Results and discussion

Computational modelling of 1bX_2 (X = Cl, Br, I)

In anticipation of the experimental work, DFT (GGA PBE-D3) calculations were used to evaluate the parameters relevant to the ability of the halogenated derivatives of **1b** to act as ChB donors or acceptors, as well as to model their expected macrocyclic tetramers to gauge the stability of the Te···O ChBs formed from such building blocks. The results are compiled in Table 1, the maxima of potential (V_{max}) on the two electrophilic regions on tellurium of the 10^{-3} a.u. isosurface of electron density (Fig. 1) increase with respect to **1b**. The effect is more intense in the region antipodal to carbon (54%) than trans to nitrogen (11%), making the two maxima of nearly equal magnitude. This suggests that, different from **1b**, predominantly electrostatic ChBs would have little preference for being trans to either element. However, there is little difference of V^N_{max} along the Cl, Br, I series and no change for V^C_{max}.

Consistently in all four cases, **1b** and **1b**X_2 (X = Cl, Br, I), the HOMO is a π molecular orbital with a prominent contribution from the oxygen atom, and the LUMO has a substantial contribution from the Te–N σ antibonding interaction. Both HOMO and LUMO descend in energy upon halogenation and the gap decreases, but the orbital energies are nearly insensitive to the nature of the halogen X.

The structures of the macrocyclic tetramers (**1b**X_2)$_4$ and **1b**$_2$(**1b**X_2)$_2$ were modelled considering two possible geometric arrangements: chair, and boat (Fig. 2), because such conformers have been structurally characterized for the **1** family.[1,2] The resulting assemblies were used to estimate the thermodynamic parameters of aggregation (Table 2). The results parallel the previous observations made on **1b**Cl_2, as the tetra-halogenated hetero-tetramers are more stable than the octa-halo homo-tetramers. Steric hindrance causes significant distortion of the boat conformation of the tetramers. However, unlike in **1b**$_2$(**1b**Cl_2)$_2$, the heavier analogues **1b**$_2$(**1b**Br_2)$_2$ and **1b**$_2$(**1b**I_2)$_2$ prefer the boat conformation.

Reactions of Iso-tellurazole *N*-oxides with iodine and bromine

The reaction of **1b** with iodine was conducted by slow (3 days) diffusion of dehydrated I_2 vapor into CH_2Cl_2 or CCl_4 solutions of the heterocycle, under a N_2 atmosphere. The product,

Table 1 DFT analysis (AMS, GGA PBE-D3, all-electron TZ2P, ZORA, gas phase) of selected iso-tellurazole *N*-oxides: V_{max} (kJ mol^{-1}) of the chalcogen electrophilic regions on the 10^{-3} a.u. iso-density surface and Frontier orbital energies (eV)

Model	V^C_{max}	V^N_{max}	E_{HOMO}	E_{LUMO}
1b	63	92	−4.95	−3.11
1bCl_2	97	102	−5.65	−4.05
1bBr_2	97	100	−5.66	−4.10
1bI_2	97	99	−5.66	−4.17
2	74	123	−5.4	−3.4
2Cl_2	102	147	−6.1	−4.3
7	45	108	−5.4	−3.0
3-Cl-7	58	126	−5.6	−3.2
3-Cl-7Cl_2	89	139	−6.3	−4.6

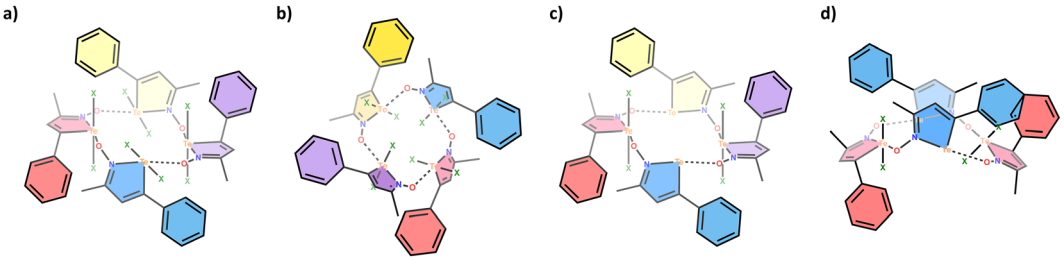

Fig. 2 Structures of all tetramers used in the evaluation of the thermodynamics of aggregation (X = Cl, Br, I). (a) $(\mathbf{1bX_2})_4$ chair, (b) $(\mathbf{1bX2})_4$ boat, (c) $\mathbf{(1b)_2(1bX2)_2}$ chair, (d) $\mathbf{(1b)_2(1bX2)_2}$ boat.

Table 2 DFT-(AMS, GGA PBE-D3, all-electron TZ2P, ZORA, gas phase) thermodynamic parameters of aggregation for the tetramers of **1b**, **1b**Br_2 and **1b**I_2.[7]

Model	ΔZPE [10^{-2} eV]	ΔH [kJ mol^{-1}]	ΔS [J mol^{-1} K^{-1}]	$\Delta G_{298.15K}$ [kJ mol^{-1}]
$\mathbf{1b}_4$ chair	2.72	−261.6	−676.4	−59.8
$(\mathbf{1b}Br_2)_4$ chair	7.35	−265.5	−733.3	−46.8
$(\mathbf{1b}Br_2)_4$ boat (distorted)	7.62	−292.8	−657.9	−55.2
$\mathbf{1b}_2(\mathbf{1b}Br_2)_2$ chair	10.88	−306.3	−700.9	−97.4
$\mathbf{1b}_2(\mathbf{1b}Br_2)_2$ boat	10.61	−308.0	−693.0	−101.6
$\mathbf{1b}_2(\mathbf{1b}I_2)_2$ chair	10.34	−306.7	−699.8	−98.1
$\mathbf{1b}_2(\mathbf{1b}I_2)_2$ boat	10.61	−317.5	−705.5	−107.1
$(\mathbf{1b}I_2)_4$ chair	5.17	−248.8	−787.8	−13.9
$(\mathbf{1b}I_2)_4$ boat (distorted)	7.07	−277.6	−756.5	−52.0
$(\mathbf{1b}Cl_2)_4$ chair	7.89	−269.3	−711.8	−57.1
$\mathbf{1b}_2(\mathbf{1b}Cl_2)_2$ chair	10.34	−292.5	−651.2	−98.3
$\mathbf{1b}_2(\mathbf{1b}Cl_2)_2$ boat	10.61	−301.6	−687.4	−96.7
$\mathbf{2}_4$ boat	7.89	−291.7	645.1	−99.3
$\mathbf{2}_4$ chair	8.16	−279.3	671.8	−79.0
$\mathbf{2}_2(\mathbf{2}Cl_2)_2$ boat	8.71	−312.6	631.5	−124.4
$\mathbf{2}_2(\mathbf{2}Cl_2)_2$ chair	9.80	−305.5	640.4	−114.6
$(\mathbf{2}Cl_2)_4$ boat	7.07	−272.7	630.4	−84.8
7 boat	7.89	−168.0	654.2	27.1
7 chair	8.44	−157.0	600.8	22.1
$\mathbf{7}_2(\text{3-Cl-7}Cl_2)_2$ boat	9.06	−201.8	600.9	−22.6
$\mathbf{7}_2(\text{3-Cl-7}Cl_2)_2$ chair	8.74	−195.4	622.1	−9.97
$(\text{3-Cl-7}Cl_2)_4$ boat	6.37	−152.7	621.4	32.55

obtained as red crystals from CCl_4, consists of the hetero-tetramers $\mathbf{1b}_2(\mathbf{1b}I_2)_2$.‡ As anticipated, $\mathbf{1b}_2$ and $\mathbf{1b}I_2$ occupy alternating positions in the macrocycle, but the ring displays the boat conformation (Fig. 3), unlike the chair structure of $\mathbf{1b}_2(\mathbf{1b}Cl_2)_2$. The Te···O ChB distances are longer than in $\mathbf{1b}_2(\mathbf{1b}Cl_2)_2$, consistent with weaker ChB interactions due to the smaller V^{N}_{max} and larger steric bulk around tellurium in $\mathbf{1b}I_2$. Within the $\mathbf{1b}_2(\mathbf{1b}Cl_2)_2$ macrocycle, d(Te1···O4) is shorter than d(Te2···O1), as the stronger ChBs are made between Te^{IV} and the oxygen of the non-halogenated molecule. The iodinated compound $\mathbf{1b}_2(\mathbf{1b}I_2)_2$ is very sensitive to moisture, which precluded obtaining satisfactory elemental analyses and mass spectra; instead, the anion HI_3^- was detected by ESI-MS (Fig. S2).

‡ The accuracy of this structure is limited because of the poor quality of the crystal. Several attempts were made to obtain better samples. A second crystal was grown from chloroform (Table S1 and Fig. S1) but it did not provide any improvement. Nevertheless, the structures unambiguously show the atom connectivity.

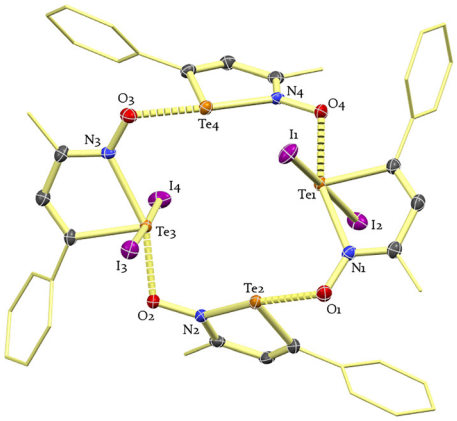

Fig. 3 Molecular structure in the crystal of $\mathbf{1b}_2(\mathbf{1b}I_2)_2$. Hydrogen atoms omitted for clarity; 50% displacement ellipsoids. Distances (Å): Te1–O4 2.100(4), Te2–O1 2.206(4), Te3–O2 2.111(4), Te4–O3 2.174(5), Te1–N1 2.315(5), Te2–N2 2.214(5), Te3–N3 2.321(5), Te4–N4 2.220(5), Te1–C1 2.124(6), Te2–C11 2.103(7), Te3–C21 2.125(6), Te4–C31 2.096(5), Te1–I1 2.9197(6), Te3–I3 2.9031(6), Te1–I2 2.8687(6), Te3–I4 2.8788(6). Dihedral angles (°): N1–Te1–O4 157.8(2), N2–Te2–O1 164.2(2), N3–Te3–O2 159.5(2), N4–Te4–O3 166.0(2).

Attempts to prepare the brominated analogue $\mathbf{1b}_2(\mathbf{1b}Br_2)_2$ by reaction with bromine or tetraalkylammonium tribromide salts[14] were frustrated by adventitious moisture, which resulted in HBr adducts, under all attempted conditions. The crystalline product from the reaction of $[Me_4N]Br_3$ with **1b** features $H\mathbf{1b}Br_3$ co-crystallized with $CHCl_3$ and one equivalent of $[Me_4N]Br$, forming Te···Br^- ChBs (Fig. 4a). Using alkyl ammonium cations with longer hydrocarbon chains (ethyl and *n*-butyl) led to the separation of oily phases. Attempts to remove $[Me_4N]Br$ from the $[Me_4N]Br$ co-crystals by filtration of their CH_3CN solutions through silica gel columns were insufficient; instead, they yielded crystals of $H\mathbf{1b}Br_3{\cdot}[Me_4N]Br$ and $(H\mathbf{1b}Br_3)_2{\cdot}[Me_4N]Br$ (Fig. 4b). These structures have Br^- chelated by a hydrogen bond and a ChB to tellurium, with 1 : 1 and 1 : 2 stoichiometries. This unusual feature may explain the strong affinity of the $(H\mathbf{1b}Br_2)^+$ moiety for the anion. However, these ChBs are significantly longer than the 3.0 Å typical of Te–Br–Te bridges.[27,28] Pure $H\mathbf{1b}Br_3$ was isolated by elution through a two-centimeter layer of a CaO and SiO_2 mixture (10% w/w). The compound, recrystallized from CH_2Cl_2, consists of large prismatic dark red crystals. The same species was also obtained

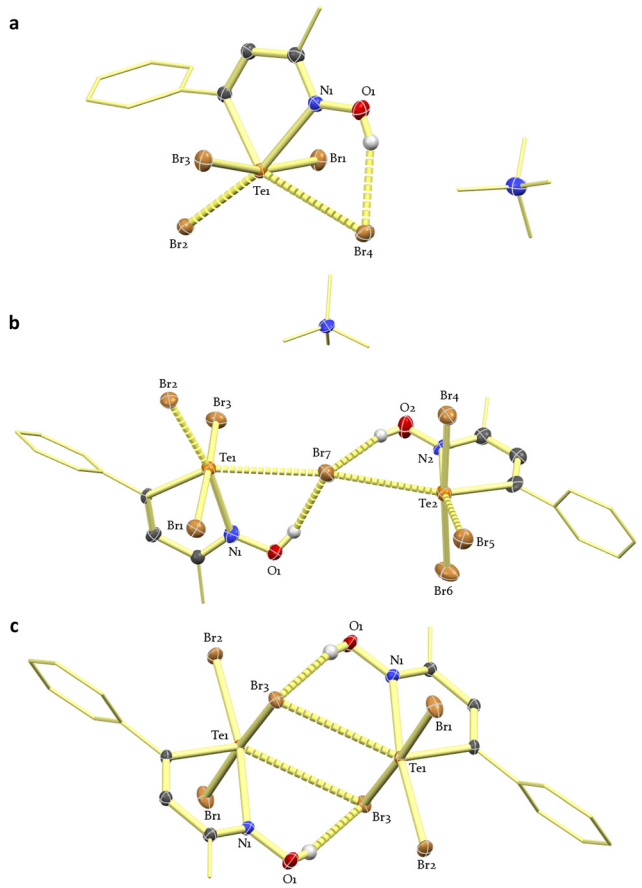

Fig. 4 Molecular structures in the crystal of: (a) H**1b**Br_3·$[Me_4N]Br$·$CHCl_3$. Distances (Å): Te1–N1 2.365(4), Te1–Br1 2.6347(6), Te1–Br2 2.6065(6), Te1–Br3 2.7048(6), Te1–Br4 3.3735(6), Te1–C1 2.165(4). Dihedral angles (°): Br3–Te1–Br1 168.80(2), Br3–Te1–Br2 93.85(2), Br1–Te1–Br2 93.66(2), Br1–Te1–C1 85.8(1), Br2–Te1–C1 93.6(1), Br3–Te1–C1 85.4(1). (b) $(H\mathbf{1b}Br_3)_2$·$[Me_4N]Br$. Distances (Å): Te1–N1 2.35(2), Te1–Br1 2.706(2), Te1–Br2 2.601(2), Te1–Br3 2.651(3), Te1–Br7 3.438(3), Te1–C1 2.16(2), Te2–N2 2.42(2), Te2–Br4 2.609(3), Te2–Br5 2.566(3), Te2–Br6 2.730(3), Te2–Br7 3.627(3). Te2–C11 2.19(2). Dihedral angles (°): Br3–Te1–Br1 170.51(8), Br3–Te1–Br2 91.61(7), Br1–Te1–Br2 94.81(7), Br1–Te1–C1 86.3(4), Br2–Te1–C1 95.2(4), Br3–Te1–C1 86.2(4), Br6–Te2–Br4 174.85(9), Br6–Te2–Br5 90.13(8), Br4–Te2–Br5 91.68(8), Br6–Te2–C11 84.1(5), Br4–Te2–C11 91.0(5), Br5–Te2–C11 95.5(5). (c) H**1b**Br_3 highlighting the dimeric arrangement. Distances (Å): Te1–N1 2.407(1), Te1–Br1 2.5721(4), Te1–Br2 2.5498(3), Te1–Br3 2.8060(4), Te1–C1 2.147(1), Te1–Br3 3.5897(4). Dihedral angles (°): Br3–Te1–Br1 174.19(1), Br3–Te1–Br2 90.37(1), Br1–Te1–Br2 95.03(1), Br1–Te1–C1 91.36(4), Br2–Te1–C1 94.35(4), Br3–Te1–C1 86.07(4).

by reaction of **1b** with an excess of Br_2(l) in CCl_4 or $CHCl_3$. **Caution:** although simpler, this method requires more precautions due to the reactivity and volatility of elemental bromine; either solvent is equally effective. Single-crystal X-ray diffraction showed that H**1b**Br_3 is isostructural to the previously known H**1b**Cl_3, with minor differences attributable to the size of the halogen (Fig. 4c). The unit cell axes are longer by 1.0%, 2.8% and 3.8%, respectively for *a*, *b* and *c*; while α and γ are unchanged, β decreases by 0.7%; and the unit-cell volume is 7% greater. Here, the molecules are organized in chalcogen-bonded pairs formed by the $[Te–X]_2$ supramolecular synthon.[29] Scaled to the respective sum of van der Waals radii, the ChB Te···Br distance (92%) is nearly equal to Te···Cl (93%), which suggests the ChBs to these halides are similar in strength.

Attempts to remove HBr from H**1b**Br_3 by reaction with bases were unsuccessful. No reaction was detected by ^{1}H NMR with $NaNH_2$ or NaOMe; LDA and *n*BuLi yielded intractable oily phases. Proton-sponge in THF yielded co-crystals of the protonated base with H**1b**Br_3 (Fig. S5) or the reduced H**1b**Br (Fig. S7). These products allowed a straighforward comparison of the structures of H**1b**Br_3 and H**1b**Br. The Te–N bond distance is longer in the brominated molecule by 0.131 Å, likely due to the increased steric hindrance around the tellurium atom.

The resistance to deprotonation of the halogenated products of **1b** was unexpected. By contrast, the experimental pK_a of **1b**H^+ (−3.2) is similar to that of protonated dialkylethers.[3] The DFT-calculated gas-phase proton affinities of **1b**X^- and **1b**X_3^- (Table 3, X = Cl, Br, I) fall within the range (−1229 to −1296 kJ mol^{-1}). There are small variations within the series; the proton affinity magnitude of H**1b**X_3 is on average 4% greater than for **1b**X, and decreases slightly from Cl to I. These values are more exothermic than the −1028 kJ mol^{-1} of proton sponge from experimental and computational evaluations;[30] and it is likely that the stability of the protonated compounds is further enhanced by the contribution of lattice energy, as well as hydrogen and chalcogen bonding interactions throughout their lattices.

Chlorination of benzo-1,2-chalcogenazole 2-oxides

Attempts were made to extend the halogenation study to the annulated derivatives **2** and **7**. Given the low solubilities of these compounds and the complications observed in the reactions of **1b** with Br_2 and I_2, these experiments were restricted to the chlorination.

Addition of SO_2Cl_2 to dilute solutions of **7** in chlorobenzene yielded H(3-Cl-7)Cl, the HCl adduct of the heterocycle chlorinated at carbon 3, instead of selenium. Its crystal structure (Fig. 5a) features a nearly coplanar (0.577 Å interplanar separation) dimer formed by hydrogen bonding between the Cl atoms and the proton of the heterocycle. Increasing the concentration of **7** to 67 mM succeeded in oxidizing the selenium atom, producing H(3-Cl-7)Cl_3. This species crystallizes forming dimers through Se···Cl ChBs, and OH···Cl hydrogen bonds (Fig. 5b). The most significant difference between these structures is in the Se–N distance, from 2.105(2) to 2.360(2) Å, *cf.* $\sum r_{cov}$ = 1.91 Å, $\sum r_{vdW}$ = 3.45 Å.

Table 3 Calculated thermodynamic parameters (AMS, GGA, PBE-D3, ZORA, all-electron TZ2P, gas phase) of the protonation of H**1b**X_3 compared to their H**1b**X counterparts

Model	ΔZPE [10^{-2} eV]	Δ*H* [kJ mol^{-1}]	Δ*S* [J mol^{-1}K^{-1}]	$\Delta G_{298.15K}$ [kJ mol^{-1}]
H**1b**Cl_3	32.9	−1274.1	−88.5	−1247.8
H**1b**Cl	32.9	−1325.1	−99.4	−1295.5
H**1b**Br_3	32.7	−1270.6	−116.9	−1235.7
H**1b**Br	33.5	−1320	−100.2	−1290.2
H**1b**I_3	31.8	−1264.1	−116.7	−1229.3
H**1b**I	32.9	−1314.2	−99.2	−1284.6

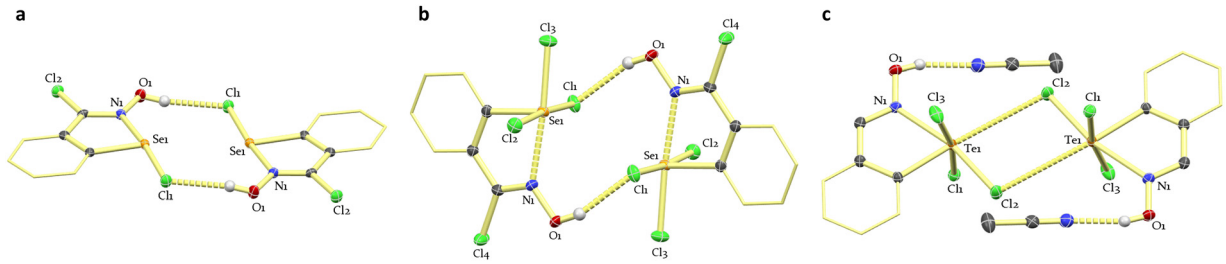

Fig. 5 Molecular structure in the crystal of: (a) H(3-Cl-**7**)Cl. Distances (Å): Se–Cl1 2.4169(7), Se–C1 1.916(2), Se···N 2.105(2). Bond angles θ (°): Cl1–Se–N 174.79(6), Cl1–Se–C1 94.81(7), C1-Se–N 80.13(9). (b) H(3-Cl-**7**)Cl_3. Distances (Å): Se1–N1 2.360(2), Se1–Cl1 2.5530(5), Se1–Cl2 2.2690(5), Se1–Cl3 2.2198(5), Se1–C1 1.961(2). Dihedral angles (°): Cl1–Se1–Cl2 174.80(2), Cl1–Se1–Cl3 92.02(2), Cl2-Se1–Cl3 93.17(2), Cl1–Se1–C1 84.50(5), Cl2-Se1–C1 94.58(5), Cl3-Se1–C1 97.65(5). (c) Molecular Structure in the crystal of H**2**Cl_3·CH_3CN. Distances (Å): Te1–N1 2.398(3), Te1–Cl1 2.528(1), Te1–Cl2 2.421(1), Te1–Cl3 2.472(1), Te1–Cl2* 3.764(2), Te1–C1 2.125(4). Dihedral angles (°): Cl3–Te1–Cl1 169.89(4), Cl3–Te1–Cl2 94.05(4), Cl1–Te1–Cl2 92.84(4), Cl3–Te1–C1 86.5(1), Cl2–Te1–Cl1 92.84(4), C1–Te1–Cl1 85.8(1). Cl3–Te1–Cl2* 72.00(3). Cl2–Te1–Cl2* 73.83(3). Cl1–Te1–Cl2* 117.14(3). Cl1–Te1–Cl2* 153.4(1).

The reaction of **2** with SO_2Cl_2 did not proceed in chlorobenzene because of the low solubility of the heterocycle. Instead, the protonated form H**2**Cl was solubilized in a MeCN/CCl_4 mixture and reacted with 2 eq. of SO_2Cl_2, producing H**7**Cl_3. Crystals of this product grew from MeCN:CH_2Cl_2 (1% v/v). Their structure confirmed halogenation of the Te atom, but the hydrogen at position 3 remained intact. The molecules are arranged in dimers linked by Te···Cl ChBs and form hydrogen bonds to molecules of MeCN (Fig. 5c).

It is natural that **2** is easier to chlorinate than **7**, but activation at position 3 only in the case of the selenium compound is unusual. Nevertheless, this finding offers a new opportunity to enhance the ChB donor ability of the chalcogen atom. The $V_{max}^{C,N}$ at the electrophilic regions, measured at the 10^{-3} a.u. isodensity surface, of **2** and **7** and their chlorinated derivatives are compiled in Table 1. In all cases, halogenation enhances the positive electrostatic potential at the electrophilic regions on the chalcogen atom. The comparison reveals that halogenation of the heterocycle has an enhancement effect comparable to the oxidation of the chalcogen. The combination of both effects in 3-Cl-7Cl_2 might result in a ChB donor as good as **1b**. Modelling for the hypothetical tetramers of **7** and its halogenated derivatives (Table 2) indicates that the homotetramers $\mathbf{7}_4$ and $(3\text{-Cl-}\mathbf{7}Cl_2)_4$ would not be stable at ambient temperature, but $\mathbf{7}_2(3\text{-Cl-}\mathbf{7}Cl_2)_2$ would be stable. However, to demonstrate and apply these findings, it is necessary to modify the structure of the benzoannulated chalcogenazole oxides to enhance their solubility and reactivity.

Experimental

DFT calculations

All calculations were performed using the AMS suite (v 2023.102-2025.102).[31] All structures were optimized using DFT with the exchange–correlation functionals of Perdew, Burke and Ernzerhof[32] and corrected for dispersion with a triple-ζ all-electron basis set[33] with two polarization functions each applying zeroth-order regular approximation formalism.[34–36] All frequency calculations were performed to ensure that each geometry was at an actual minimum in the potential energy surface and to derive the corresponding thermodynamic parameters.

Materials and methods

Air-sensitive reactions and materials were handled under an inert atmosphere of nitrogen. Organic solvents were dehydrated using the appropriate dehydrating agents under nitrogen. **1b**, **7** and **2** were prepared according to the methods in literature.[2,4,25] Tetramethylammonium tribromide (TMATB) was prepared as published.[37]

Nuclear magnetic resonance

All spectra obtained were done using a deuterated solvent. The spectra were obtained using Bruker Avance 600 MHz (Bruker 5 mm Broad Band Observe probe) spectrometers at 287.5 K unless otherwise noted. The ^{1}H and ^{13}C spectra were processed using the Bruker TopSpin 4.2.0 software package. The ^{1}H-NMR and ^{13}C-NMR spectra were referenced to the resonances of the residual ^{1}H and the natural ^{13}C in the deuterated solvent. The low solubility of the samples precluded observation of the ^{77}Se, and ^{125}Te resonances.

Electrospray ionization mass spectrometry

Mass spectra of H**1**Br_3 and H**1b**I_3 were obtained in the negative on a Waters/Micromass Quattro Ultima Global TOF mass spectrometer functioning in the negative ion mode. The samples were dissolved in dichloromethane and diluted with MeOH.

Crystallography

Suitable crystals of each compound were mounted on nylon loops (Hampton, California) or MiTeGen micromounts (Ithaca, New York) with Paratone-N oil on a Bruker APEX-II CCD, STOE IPDS II or BRUKER D8 VENTURE diffractometer. The crystals were kept at 100.00 K during data collection. Using Olex2,[38] the structures were solved with the Olex2.Solv[39] structure solution program using charge flipping and refined with the SHELXL refinement package using least squares minimization.[40]

Synthetic procedures

()H1bBr$_3$)$_2$. Method 1. Compound **1b** (52.5 mg) was suspended in anhydrous MeOH (2 mL) under an inert atmosphere. TMATB was dissolved in anhydrous MeOH (115 mg in 2 mL) and added dropwise with stirring. The mixture was stirred for

20 minutes at room temperature, and the solvent was evaporated to dryness under reduced pressure. The product was extracted with CH_2Cl_2 and precipitated from hexanes, yielding a light-yellow powder. The light-yellow powder was redissolved in MeCN and filtered through a 2 cm-thick layer of activated silica to remove TMAB. The solution volume was reduced under vacuum, redissolved in 2 mL CH_2Cl_2 and precipitated by addition of hexanes. Method 2. Two drops of Br_2(l) were added to a solution of **1b** in CCl_4 (**caution**: hepatotoxic solvent). Yield: 48%; mp: 140–145 °C (d); ^{1}H-NMR (600 MHz, $CDCl_3$) δ 7.57–7.46 (m, 5H), 6.51 (s, 1H), 2.33 (s, 3H); ^{13}C NMR (600 MHz, $CDCl_3$) δ 153.6, 134.9, 130.9, 130.5, 128.6, 128.3, 127.9, 16.2; IR: 3646, 2924, 2853, 2364, 2093, 1970, 1456, 1231, 1157, 888, 832, 715, 683, 601, 568 cm^{-1}; analysis (calcd, found for $C_{14}H_{22}Br_4N_2OTe$): C (24.67, 24.09), H (3.25, 2.82), N (4.11, 3.65); HRMS (*m*/*z*): $[M–H]^-$ calcd for $C_{10}H_{10}NO[^{130}Te][^{81}Br]_3$, 531.7246; found, 531.7246.

1b$_2$(1bI$_2$)$_2$. Compound **1b** (14.7mg) was dissolved in 3 mL of CCl_4 (**caution**: hepatotoxic solvent) in a test tube under a N_2 atmosphere and inserted into a larger tube containing an excess of I_2(s). Once the larger tube was closed, vapor of I_2 was allowed to diffuse into the solution over 48 hours. Simultaneously, the solvent evaporated slowly, depositing small red crystals on the walls of the inner tube. Yield 42%; mp: 120–126 °C (d); ^{1}H-NMR (600MHz, $CDCl_3$) δ 7.45–7.25 (m, 5H), 7.03 (s, 1H), 1.78 (s, 3H). IR: 2961, 2919, 2850, 2360, 1573, 1490, 1440, 1372, 1339, 1261, 1219, 1090, 1026, 925, 905, 866, 800, 758, 691, 614, 579, 531; tHRMS (*m*/*z*): [M + I] calcd for $C_{10}H_9NOI_3[^{130}Te]$ 669.6886, found 669.688.

H(3-Cl-7)Cl$_3$. This compound was synthesized in chlorobenzene which was freshly filtered through 100 mesh activated alumina. A 0.0668M solution of **7** was prepared by gently heating the solvent, allowed to cool down and layered on top of a solution containing 2 eq. of SO_2Cl_2 in CCl_4 (**caution**: hepatotoxic solvent). The sample was stored at −30 °C and pale yellow crystals formed after 24 hours. The compound was identified by single-crystal X-ray diffraction; its spectroscopic characterization was hindered by its low solubility.

H2Cl$_3$. The above method was adapted for the chlorination of H2Cl (previously prepared in MeOH from **2** and 0.5M HCl). A 0.129M solution of the hydrochloride in CH_3CN was added to 2 eq. SO_2Cl_2 in CCl_4 (**caution**: hepatotoxic solvent). The solution was concentrated under vacuum to dryness producing a light-yellow solid which was redissolved in MeCN:CH_2Cl_2 (1% v/v). Slow evaporation under N_2 produced small light-yellow crystals. The compound was identified by single-crystal X-ray diffraction; its spectroscopic characterization was hindered by its low solubility.

Summary and conclusions

Motivated by the goal to enhance the ChB acceptor ability of iso-chalcogenazole *N*-oxides, these investigations expand the findings from previous work on the reactions of halogens with such supramolecular building blocks. DFT calculations confirmed that halogenation increases V_{max} at the electrophilic regions on the surface of the chalcogen atom, enhancing its ChB-donor ability. While the effect of halogenation is very clear, the calculations show only small differences between the derivatives of chlorine, bromine and iodine. The concomitant polarization of oxygen atoms and steric hindrance counter the ChB-acceptor strength, the result is a thermodynamic preference for formation of hetero-tetramers **1b**$_2$(**1b**X$_2$)$_2$ (X = Cl, Br, I).

Experimentally, while $[R_4N]Br_3$ salts were effective brominating agents, the isolated products were consistently protonated, *e.g.* H**1b**Br_3 and could not be turned into the respective free bases. This likely is a consequence of the strong ChB interaction with the bromide anion, which also stabilized co-crystals such as $[Me_4N]Br$. In contrast, the reaction of **1b** with I_2 yielded the expected hetero-tetramer **1b**$_2$(**1b**I$_2$)$_2$, which has the typical macrocyclic structure assembled by ChB from iso-tellurazole *N*-oxides.

Protonation was also observed when **2** and **7** reacted with SO_2Cl_2. Compound **2** reacted as usual, forming H2Cl_3; but with **7**, chlorination occurred at the heterocycle, yielding H(3-Cl-7)Cl; an excess of reagent was required to chlorinate the chalcogen and produce H(3-Cl-7)Cl_3. The reaction at position 3 is particularly interesting. DFT calculations indicate that this is a viable alternative to chalcogen halogenation to enhance the electrophilicity of the chalcogen. More importantly, it opens a potential route for further functionalization of the heterocycle by catalytic coupling.[17] Such modifications could be useful to improve solubility, modulate ChB strength or facilitate the synthesis of other organic heterocycles.[41]

Author contributions

PLM: conceptualization, investigation, methodology, visualization, writing – original draft; MWZ: investigation, visualization, writing – review & editing; JZW: conceptualization, investigation, methodology; PCH: investigation, methodology, supervision; IVB: conceptualization, funding acquisition, methodology, project administration, resources, supervision, writing – review & editing.

Conflicts of interest

There are no conflicts to declare.

Data availability

The data supporting this article have been included as part of the supplementary information (SI). Supplementary information: spectroscopic data, Cartesian coordinates of calculated molecul crystallographic information files (already deposited at the CCDC). Raw crystallographic data; ^{1}H and ^{13}C NMR spectra; mass spectra; results of combustion elemental analyses; output files of DFT calculations, can be made available upon request. See DOI: https://doi.org/10.1039/d5nj03688g.

CCDC 2348773, 2311589, 2327455, 2311414, 2310895, 2311624, 2311572, 2327465, 2309983 and 2309984 contain the supplementary crystallographic data for this paper.[42a–j]

Acknowledgements

We gratefully acknowledge the support of the Natural Sciences and Engineering Research Council (NSERC) of Canada (IVB: DG; PCH: PGSD) and Ontario (JZW: OGF). This research was enabled in part by support provided by the Shared Hierarchical Academic Research Computing Network (SHARCNET, https://www.sharcnet.ca) and the Digital Research Alliance of Canada (alliancecan.ca).

Notes and references

1 J. Kübel, P. J. W. Elder, H. A. Jenkins and I. Vargas-Baca, *Dalton Trans.*, 2010, **39**, 11126–11128.
2 P. C. Ho, P. Szydlowski, J. Sinclair, P. J. W. Elder, J. Kübel, C. Gendy, L. M. Lee, H. Jenkins, J. F. Britten, D. R. Morim and I. Vargas-Baca, *Nat. Commun.*, 2016, **7**, 11299.
3 P. C. Ho, L. M. Lee, H. Jenkins, J. F. Britten and I. Vargas-Baca, *Can. J. Chem.*, 2016, **94**, 453–457.
4 P. C. Ho, J. Rafique, J. Lee, L. M. Lee, H. A. Jenkins, J. F. Britten, A. L. Braga and I. Vargas-Baca, *Dalton Trans.*, 2017, **46**, 6570–6579.
5 J. Wang, P. C. Ho, J. F. Britten, V. Tomassetti and I. Vargas-Baca, *New. J. Chem.*, 2019, **43**, 12601–12608.
6 P. C. Ho, R. Bui, A. Cevallos, S. Sequeira, J. F. Britten and I. Vargas-Baca, *Dalton Trans.*, 2019, **48**, 4879–4886.
7 P. C. Ho, J. Lomax, V. Tomassetti, J. F. Britten and I. Vargas-Baca, *Chem. – Eur. J.*, 2021, **27**, 10849–10853.
8 J. Wang, P. C. Ho, M. G. J. Craig, A. Cevallos, J. F. Britten and I. Vargas–Baca, *Chem. – Eur. J.*, 2024, **30**, e202302538.
9 C. B. Aakeroy, D. L. Bryce, G. R. Desiraju, A. Frontera, A. C. Legon, F. Nicotra, K. Rissanen, S. Scheiner, G. Terraneo, P. Metrangolo and G. Resnati, *Pure Appl. Chem.*, 2019, **91**, 1889–1892.
10 N. Biot and D. Bonifazi, *Coord. Chem. Rev.*, 2020, **413**, 213243.
11 N. Biot and D. Bonifazi, *Chem. – Eur. J.*, 2017, **24**, 5439–5443.
12 A. Kremer, A. Fermi, N. Biot, J. Wouters and D. Bonifazi, *Chem. – Eur. J.*, 2016, **22**, 5665–5675.
13 P. Scilabra, G. Terraneo and G. Resnati, *Acc. Chem. Res.*, 2019, **52**, 1313–1324.
14 W. Yang, R. Jiang, C. Liu, B. Yu, X. Cai and H. Wang, *Cryst. Growth Des.*, 2021, **21**, 6497–6503.
15 B. J. Eckstein, L. C. Brown, B. C. Noll, M. P. Moghadasnia, G. J. Balaich and C. M. McGuirk, *J. Am. Chem. Soc.*, 2021, **143**, 20207–20215.
16 D. Romito, E. Fresta, L. M. Cavinato, H. Kählig, H. Amenitsch, L. Caputo, Y. Chen, P. Samorì, J. Charlier, R. D. Costa and D. Bonifazi, *Angew. Chem., Int. Ed.*, 2022, **61**, e202202137.
17 Z. N. Scheller, J. Schulte, C. Wölper and G. Haberhauer, *Chem. – Eur. J.*, 2025, e01571.
18 S. Benz, J. López-Andarias, J. Mareda, N. Sakai and S. Matile, *Angew. Chem., Int. Ed.*, 2017, **56**, 812–815.
19 S. Benz, A. I. Poblador-Bahamonde, N. Low-Ders and S. Matile, *Angew. Chem., Int. Ed.*, 2018, **57**, 5408–5412.
20 L. Vogel, P. Wonner and S. M. Huber, *Angew. Chem., Int. Ed.*, 2018, **58**, 1880–1891.
21 D. Jovanovic, M. P. Mohanan and S. M. Huber, *Angew. Chem., Int. Ed.*, 2024, **63**, e202404823.
22 L. M. Lee, M. Tsemperouli, A. I. Poblador-Bahamonde, S. Benz, N. Sakai, K. Sugihara and S. Matile, *J. Am. Chem. Soc.*, 2019, jacs.8b12554.
23 A. V. Jentzsch, D. Emery, J. Mareda, S. K. Nayak, P. Metrangolo, G. Resnati, N. Sakai and S. Matile, *Nat. Commun.*, 2012, **3**, 905.
24 A. V. Jentzsch and S. Matile, *J. Am. Chem. Soc.*, 2013, **135**, 5302–5303.
25 P. C. Ho, V. Tomassetti, J. F. Britten and I. Vargas-Baca, *Inorg. Chem.*, 2021, **60**, 16726–16733.
26 A. F. Cozzolino, I. Vargas-Baca, S. Mansour and A. H. Mahmoudkhani, *J. Am. Chem. Soc.*, 2005, **127**, 3184–3190.
27 S. M. Närhi, J. Kutuniva, M. K. Lajunen, M. K. Lahtinen, H. M. Tuononen, A. J. Karttunen, R. Oilunkaniemi and R. S. Laitinen, *Spectrochim. Acta, Part A*, 2014, **117**, 728–738.
28 A. L. Hector, A. Jolleys, W. Levason and G. Reid, *Dalton Trans.*, 2012, **41**, 10988.
29 A. F. Cozzolino, P. J. W. Elder and I. Vargas-Baca, *Coord. Chem. Rev.*, 2011, **255**, 1426–1438.
30 M. Mathew, R. Puchta and R. Thomas, *Comput. Theor. Chem.*, 2024, **1233**, 114477.
31 E. J. Baerends, N. F. Aguirre, N. D. Austin, J. Autschbach, F. M. Bickelhaupt, R. Bulo, C. Cappelli, A. C. T. van Duin, F. Egidi, C. F. Guerra, A. Förster, M. Franchini, T. P. M. Goumans, T. Heine, M. Hellström, C. R. Jacob, L. Jensen, M. Krykunov, E. van Lenthe, A. Michalak, M. M. Mitoraj, J. Neugebauer, V. P. Nicu, P. Philipsen, H. Ramanantoanina, R. Rüger, G. Schreckenbach, M. Stener, M. Swart, J. M. Thijssen, T. Trnka, L. Visscher, A. Yakovlev and S. van Gisbergen, *J. Chem. Phys.*, 2025, **162**, 162501.
32 J. P. Perdew, K. Burke and M. Ernzerhof, *Phys. Rev. Lett.*, 1996, **77**, 3865–3868.
33 E. V. Lenthe and E. J. Baerends, *J. Comput. Chem.*, 2003, **24**, 1142–1156.
34 E. V. Lenthe, J. G. Snijders and E. J. Baerends, *J. Chem. Phys.*, 1996, **105**, 6505–6516.
35 E. V. Lenthe, R. V. Leeuwen, E. J. Baerends and J. G. Snijders, *Int. J. Quantum Chem.*, 1996, **57**, 281–293.
36 E. V. Lenthe, A. Ehlers and E. J. Baerends, *J. Chem. Phys.*, 1999, **110**, 8943–8953.
37 F. D. Chattaway and G. Hoyle, *J. Chem. Soc., Trans.*, 1923, **123**, 654–662.
38 O. V. Dolomanov, L. J. Bourhis, R. J. Gildea, J. A. K. Howard and H. Puschmann, *J. Appl. Crystallogr.*, 2009, **42**, 339–341.
39 L. J. Bourhis, O. V. Dolomanov, R. J. Gildea, J. A. K. Howard and H. Puschmann, *Acta Crystallogr., Sect. A: Found. Adv.*, 2015, **71**, 59–75.
40 G. M. Sheldrick, *Acta Crystallogr., Sect. C: Struct. Chem.*, 2015, **71**, 3–8.
41 K. Shimada, Y. Takata, Y. Osaki, A. Moro-oka, H. Kogawa, M. Sakuraba, S. Aoyagi, Y. Takikawa and S. Ogawa, *Tetrahedron Lett.*, 2009, **50**, 6651–6653.

42 (*a*) CCDC 2348773: Experimental Crystal Structure Determination, 2025, DOI: 10.5517/ccdc.csd.cc2jv2wc; (*b*) CCDC 2311589: Experimental Crystal Structure Determination, 2025, DOI: 10.5517/ccdc.csd.cc2hlddx; (*c*) CCDC 2327455: Experimental Crystal Structure Determination, 2025, DOI: 10.5517/ccdc.csd.cc2j3x6s; (*d*) CCDC 2311414: Experimental Crystal Structure Determination, 2025; (*e*) CCDC 2310895: Experimental Crystal Structure Determination, 2025, DOI: 10.5517/ccdc.csd.cc2hl6r2; (*f*) CCDC 2311624: Experimental Crystal Structure Determination, 2025, DOI: 10.5517/ccdc.csd.cc2hlfj2; (*g*) CCDC 2311572: Experimental Crystal Structure Determination, 2025, DOI: 10.5517/ccdc.csd.cc2hlcvb; (*h*) CCDC 2327465: Experimental Crystal Structure Determination, 2025, DOI: 10.5517/ccdc.csd.cc2j3xj3; (*i*) CCDC 2309983: Experimental Crystal Structure Determination, 2025, DOI: 10.5517/ccdc.csd.cc2hjqlc; (*j*) CCDC 2309984: Experimental Crystal Structure Determination, 2025, DOI: 10.5517/ccdc.csd.cc2hjqmd.

